Active Layer-Incorporated, Spectrally Tuned Au/SiO_2 Core/Shell Nanorod-Based Light Trapping for Organic Photovoltaics

Vladan Janković,[†,⊥] Yang (Michael) Yang,[‡,⊥] Jingbi You,[‡] Letian Dou,[‡] Yongsheng Liu,[‡] Puilam Cheung,[†] Jane P. Chang,[†,§] and Yang Yang[‡,§,*]

[†]Department of Chemical Engineering, [‡]Department of Materials Science and Engineering, and [§]California NanoSystems Institute, University of California, Los Angeles, California 90095, United States. [⊥]These authors contributed equally to this work.

ABSTRACT We demonstrate that incorporation of octadecyltrimethoxysilane (OTMS)-functionalized, spectrally tuned, gold/silica (Au/SiO_2) core/shell nanospheres and nanorods into the active layer of an organic photovoltaic (OPV) device led to an increase in photoconversion efficiency (PCE). A silica shell layer was added onto Au core nanospheres and nanorods in order to provide an electrically insulating surface that does not interfere with carrier generation and transport inside the active layer. Functionalization of the Au/SiO_2 core/shell nanoparticles with the OTMS organic ligand was then necessary to transfer the Au/SiO_2 core/shell nanoparticles from an ethanol solution into an OPV polymer-compatible solvent, such as dichlorobenzene. The OTMS-functionalized Au/SiO_2 core/shell nanorods and nanospheres were then incorporated into the active layers of two OPV polymer systems: a poly(3-hexylthiophene):[6,6]-phenyl-C61-butyric acid methyl ester (P3HT:$PCB_{60}M$) OPV device and a poly[2,6-4,8-di(5-ethylhexylthienyl)benzo[1,2-*b*;3,4-*b*]dithiophene-*alt*-5-dibutyloctyl-3,6-bis(5-bromothiophen-2-yl)pyrrolo[3,4-*c*]pyrrole-1,4-dione] (PBDTT-DPP:$PC_{60}BM$) OPV device. For the P3HT:$PC_{60}BM$ polymer with a band edge of ~700 nm, the addition of the core/shell nanorods with an aspect ratio (AR) of ~2.5 (extinction peak ~670 nm) resulted in a 7.1% improvement in PCE, while for the PBDTT-DPP:$PC_{60}BM$ polymer with a band edge of ~860 nm, the addition of core/shell nanorods with an AR of ~4 (extinction peak ~830 nm) resulted in a 14.4% improvement in PCE. The addition of Au/SiO_2 core/shell nanospheres to the P3HT:$PC_{60}BM$ polymer resulted in a 2.7% improvement in PCE, while their addition to a PBDTT-DPP:$PC_{60}BM$ polymer resulted in a 9.1% improvement. The PCE and J_{sc} enhancements were consistent with external quantum efficiency (EQE) measurements, and the EQE enhancements spectrally matched the extinction spectra of Au/SiO_2 nanospheres and nanorods in both OPV polymer systems.

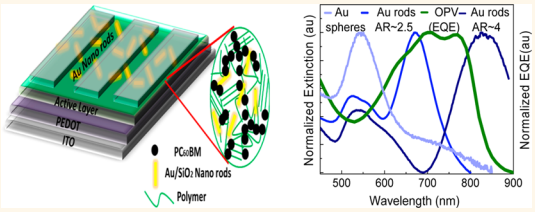

KEYWORDS: plasmonic effect · surface plasmon · organic photovoltaics · plasmonic organic photovoltaics · polymer solar cells · gold nanorods · gold nanospheres · core/shell nanostructure · silica shells · aspect ratio

Given that its active layer is amenable to simple solution processing, organic photovoltaic (OPV) technology is an inexpensive, flexible, and lightweight option for solar energy conversion. Research in organic solar cells started in the early 1980s and focused on Schottky junctions with low work function metals and p-n junctions with p-type organic semiconducting polymers and inorganic n-type semiconductors.[1−5] Interest in the field intensified after Tang *et al.* demonstrated an OPV device in 1986 with a 0.95% efficiency using organic polymers as both donors and acceptors.[6] Other breakthroughs in OPV technology came with the introduction of buckminsterfullerene (C_{60}) and its derivatives, such as [6,6]-phenyl-C_{60}-butyric acid methyl ester ($PC_{60}BM$) as n-type organic materials by Sariciftci *et al.*[7,8] and with the development of the bulk heterojunction (BHJ) by Hiramoto *et al.*[9] Seminal BHJ OPV papers using poly(2-methoxy-5(20-ethylhexyloxy)-1,4-phenylenevinylene (MEH-PPV) as the donor molecule and $PC_{60}BM$ as the acceptor molecule were published by the Heeger[10] and Friend[11] groups independently in 1995. As research in the field continued, studies revealed that the nanoscale morphology of the active layer of OPV devices was critical for optimizing their efficiency.[12,13] Numerous strategies, including solvent

* Address correspondence to yangy@ucla.edu.

Received for review July 24, 2012 and accepted April 29, 2013.

Published online April 29, 2013
10.1021/nn400246q

selection,[14−16] thermal annealing,[17] and the incorporation of various additives,[13] have led to improved active layer morphologies and consequently further improvements in photon conversion efficiencies (PCEs).[18] High carrier mobility donor polymers such as poly(3-hexylthiphene) (P3HT)[19] and low band gap polymers such as poly[2,6-4,8-di(5-ethylhexylthienyl)benzo[1,2-*b*;3,4-*b*]dithiophene-*alt*-5-dibutyloctyl-3,6-bis(5-bromothiophen-2-yl)pyrrolo[3,4-*c*]pyrrole-1,4-dione] (PBDTT-DPP), which have absorption wavelengths that extend up to ∼850 nm, have also led to PCE improvements.[20] Currently, a PCE of over 9% for single-junction OPVs has been achieved by Mitsubishi Chemical,[21] and a NREL-certified PCE of 10.6% has been achieved for tandem cells.[22,23]

Photons absorbed by an OPV device can only generate current if they are absorbed near donor−acceptor interfaces such that dissociation occurs prior to dissipative recombination. Since the carrier mobility is small in photoactive polymers (on the order of 10^{-4} $cm^2/V\cdot s$ or less), it is common to use rather thin films (100 nm or less) in order to achieve efficient carrier extraction.[24] The use of such thin layers means a significant portion of the incident photon flux remains unharvested; it also means that the light absorption efficiencies of OPV devices can be improved.

Light trapping refers to the various methods used to increase the distance over which incident photons interact with photovoltaic (PV) materials, thereby increasing the likelihood of photon absorption. From a ray-optics perspective, conventional light trapping employs total internal reflection by patterning the entrance or exit interfaces of the solar cell and redirecting the incident light into the PV active layer.[25] In thick crystalline silicon solar cells, light trapping is typically achieved with the use of patterned structures that have features on the scale of the wavelength of light;[26] however, since the active layers in organic cells have thicknesses that are far smaller than the wavelength of light, the relatively large-scale geometries used in traditional light trapping designs are not suitable for OPVs.[27] For OPV applications, light trapping techniques that rely on structures compatible with the scale of OPV films, in other words, at a scale less than 100 nm, are needed.[26]

One light trapping method that shows promise for OPV applications involves the use of noble metal (mainly gold or silver) nanoparticles.[28] Noble metal nanoparticles are capable of confining resonant photons in such a manner as to induce coherent surface plasmon oscillation of their conduction band electrons.[29] At the resonant frequency, termed the local surface plasmon resonance (LSPR), a large enhancement of the nanoparticle's light absorption and scattering properties occurs.[30] For example, a Ag nanoparticle in air has a scattering cross section that is around 10 times the geometrical cross-sectional area of the particle; hence, a substrate covered with a 10% areal density of Ag particles could ideally absorb and scatter all of the light incident on the substrate.[29] Indeed, noble metal nanoparticles deposited on the top of thin film solar cells have been shown to preferentially scatter light into the high-index substrate, leading to enhanced coupling with the underlying semiconductor and thus a reduced reflectance over a broad spectral range.[32]

Light trapping with Au and Ag nanoparticles for OPVs has been demonstrated by various groups.[33] By incorporating Au nanospheres (∼45 nm diameter) into the poly(ethylenedioxythiophene):polystyrenesulfonate (PEDOT:PSS) buffer layer of a P3HT:PC_{60}BM OPV device, Morfa *et al.* increased the PCE of the device from 1.3 to 2.2%.[33] Qiao *et al.* showed that Au nanoparticles (∼15 nm diameter) introduced into the PEDOT:PSS layer of an OPV device using poly(2-methoxy-5(20-ethylhexyloxy)-1,4-phenylenevinylene (MEH-PPV) as the active layer enhanced the PCE from 1.99 to 2.36%,[34] while Wu *et al.* demonstrated that incorporating Au nanoparticles (∼45 nm diameter) into the anodic buffer layer of a P3HT:PC_{60}BM OPV device improved the PCE from 3.57 to 4.24%.[35] More recently, Au nanoparticles (∼72 nm diameter) were deposited in the interconnecting layer of an inverted tandem polymer solar cell, resulting in a 20% increase in PCE (from 5.22 to 6.24%).[36] In all of these reports, because the plasmonic nanoparticles were inserted relatively far from the active organic layers of the OPV devices, the documented absorption enhancements arose from the light scattering properties of the Au nanoparticles and failed to exploit the near-field enhanced LSPR modes.[26] As theoretical studies have shown, embedding plasmonic nanoparticles into the active layer of an OPV device can capitalize on both the light scattering effect and the enhanced LSPR near-field.[37,38]

Currently, there are only a few reports documenting incorporation of plasmonic materials into OPV active layers. Szeremeta *et al.* showed that Cu nanoparticles (20 nm) embedded inside P3HT layers enhanced the dissociation of excitons without increasing the P3HT optical absorption.[39] Wang *et al.* demonstrated improved PCEs in three different polymer systems resulting from the incorporation of Au nanoparticles into the active layers.[40] Xue *et al.* incorporated Ag nanoparticles into the active layer of a P3HT:PC_{60}BM OPV device and found that, while their addition into the active layer significantly enhanced carrier mobility, it decreased the total extracted carrier density.[41] A potential way to address this issue is to coat the noble metal nanoparticles with a thin layer of SiO_2, rendering their surfaces insulating yet still allowing them to retain their attractive optical properties.

The frequency of light that is resonantly absorbed and scattered from a nanoparticle is another important consideration in optimizing OPV device performance.

Since different OPV polymers have different light absorption frequency bands, it is of interest to develop a light trapping technique that can be tailored to specific OPV polymers. The peak extinction frequency of noble metal nanospheres is ~520 nm and varies ~20 nm depending on the nanosphere size.[31] In Au nanorods, on the other hand, free electrons oscillate along both the long and short axes of the rod, resulting in two resonance bands: a band of wavelengths resulting from electron oscillations along the long axis, which, depending on the nanorod aspect ratio (AR) ranges between ~600 and ~900 nm, and, a second, weaker band at ~520 nm resulting from electron oscillations along the short axis (similar to nanospheres).[42] Incorporating Au nanorods of different ARs (and hence different peak extinction wavelengths) into OPV active layers can thus be utilized to achieve LSPR near-field absorption enhancements over a large range of wavelengths.

RESULTS AND DISCUSSION

In order to study the viability of this approach, Au/SiO_2 core/shell nanospheres and nanorods were incorporated into the active layers of two polymer OPV systems: broad band gap P3HT:$PC_{60}BM$ and low band gap PBDTT-DPP:$PC_{60}BM$. We hypothesized that the greatest enhancement due to the LSPR near-field would be observed in spectral regions where the OPV polymer absorbs poorly and the lowest enhancement would be observed in spectral regions where the OPV polymer absorbs efficiently. To investigate this hypothesis, EQE measurements on OPV devices with spectrally tuned Au/SiO_2 nanoparticles were performed. For the P3HT:$PC_{60}BM$ system, Au/SiO_2 nanospheres with a peak extinction of ~540 nm (matching a spectral region of high polymer absorption) and AR ~ 2.5 Au/SiO_2 nanorods with a peak extinction of ~670 nm (matching a spectral region of poor polymer absorption at the band edge of the P3HT:$PC_{60}BM$) were synthesized. For the low band gap polymer PBDTT-DPP:$PC_{60}BM$ system, Au/SiO_2 nanospheres with a peak extinction of ~540 nm (matching a spectral region of moderate polymer absorption) and AR ~ 4 Au/SiO_2 nanorods with a peak extinction of ~830 nm (matching a spectral region of poor polymer absorption at the OPV polymer band edge) were synthesized. The SiO_2 shell thickness in all samples was ~10 nm. Short circuit current (J_{sc}), open circuit voltage (V_{oc}), and external quantum efficiency (EQE) measurements were performed on the devices. Blending the Au/SiO_2 nanospheres and nanorods into the active layer resulted in enhanced J_{sc} and PCE in both the P3HT:$PC_{60}BM$ and PBDTT-DPP:$PC_{60}BM$ devices compared to the reference devices (Supporting Information, Tables S.1–S.4). Figure 1i shows the transmission electron microscopy (TEM) images of (A) Au nanospheres, (B) AR ~ 2.5 Au nanorods, (C) AR ~ 4 Au nanorods, (D) Au/SiO_2 nanospheres, (E) AR ~ 2.5 Au/SiO_2 nanorods, and (F) AR ~ 4 Au/SiO_2 nanorods. Figure 1ii shows the extinction spectra of bare Au nanospheres, AR ~ 2.5 nanorods, and AR ~ 4 nanorods in water (corresponding TEM images are A–C) plotted with the extinction spectra of Au/SiO_2 core/shell nanorods in dichlorobenzene (corresponding TEM images are D–F). Figure 1iii shows normalized extinction spectra of solutions D and E plotted with a normalized EQE spectrum of P3HT:$PC_{60}BM$, while Figure 1iv shows a normalized EQE spectrum of PBDTT-DPP:$PC_{60}BM$ plotted with normalized extinction spectra of solutions D and F. Figure 1v shows the reference and plasmonic OPV device EQE spectra for the P3HT:$PC_{60}BM$ system, while the EQE spectra of plasmonic and reference devices using the PBDTT-DPP:$PC_{60}BM$ system are shown in Figure 1vi.

The reference device EQE spectra were subtracted from the plasmonic device EQE and divided by the reference device EQE spectra in order to obtain spectral EQE enhancement percentages ($\Delta EQE\ (\%,\lambda) = (EQE_{plasmonic}\ (\%,\lambda) - EQE_{ref}\ (\%,\lambda))$. Figure 2 shows EQE enhancement factors ($\Delta EQE/EQE_{ref}$) of OPV plasmonic devices compared to reference devices plotted with the extinction spectra of Au/SiO_2 nanosphere and nanorod colloidal solutions embedded in their active layers.

EQE enhancements in both polymer systems spectrally matched the extinction spectra of the active layer-incorporated Au/SiO_2 core/shell nanospheres and nanorods. AR ~ 4 Au/SiO_2 core/shell nanorods with extinction peaks matching the band edges of the PBDTT-DPP:$PC_{60}BM$ systems showed the highest EQE enhancement factors, while Au/SiO_2 nanospheres incorporated in the P3HT:$PC_{60}BM$ system showed the lowest performance enhancement. In the low band gap polymer system, PBDTT-DPP:$PC_{60}BM$, we found that the improvement was in two spectral regions: one that matched the longitudinal oscillation mode of the Au/SiO_2 nanorods and one that matched the transverse oscillation mode of the Au/SiO_2 nanorods. The mismatch between the EQE of the P3HT:$PC_{60}BM$ polymer system and the extinction spectrum of the Au/SiO_2 nanospheres requires further investigation.

A concentration study was also conducted and revealed that OPV device performance depended on the amount of Au/SiO_2 core/shell nanospheres or nanorods incorporated into the active layer. Increasing the amount of Au/SiO_2 nanoparticles led to an initial increase in solar cell PCE. As the Au/SiO_2 concentration increased, however, a drop in device performance was observed. For the P3HT:$PC_{60}BM$ system, the optimal Au/SiO_2 nanosphere concentration was 0.4 and 0.6 mg/mL for the Au/SiO_2 nanorods; concentrations of nanospheres or nanorods greater than 2 mg/mL resulted in OPV device performance degradation. The optimum Au/SiO_2 core/shell nanosphere concentration for the PBDTT-DPP:$PC_{60}BM$ system was 0.1 and

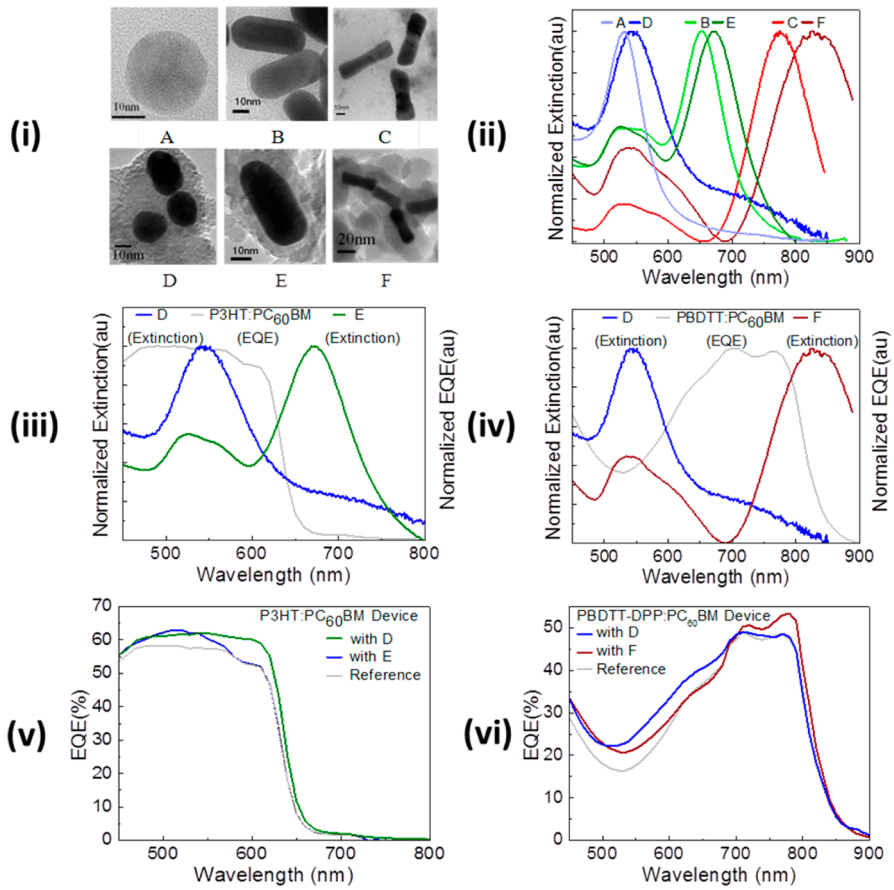

Figure 1. (i) TEM images and (ii) extinction spectra of corresponding colloidal solutions of (A) Au nanospheres in water, (B) Au/SiO_2 core/shell nanospheres in dichlorobenzene (DCB), (C) Au nanorods of AR ~ 2.5 in water, (D) Au/SiO_2 core/shell nanorods of AR ~ 2.5 in DCB, (E) Au nanorods of AR ~ 4 in water, (F) Au/SiO_2 core/shell nanorods of AR ~ 4 in DCB A–F. (iii) Normalized EQE of P3HT:PC_{60}BM plotted with normalized extinction spectra of D and E. (iv) Normalized EQE spectrum of PBDTT-DPP:PC_{60}BM devices with D and F and reference devices. (v) Reference and plasmonic OPV device EQE spectra for the P3HT:PC_{60}BM system. (vi) Reference and plasmonic OPV device EQE spectra for the PBDTT-DPP:PC_{60}BM system.

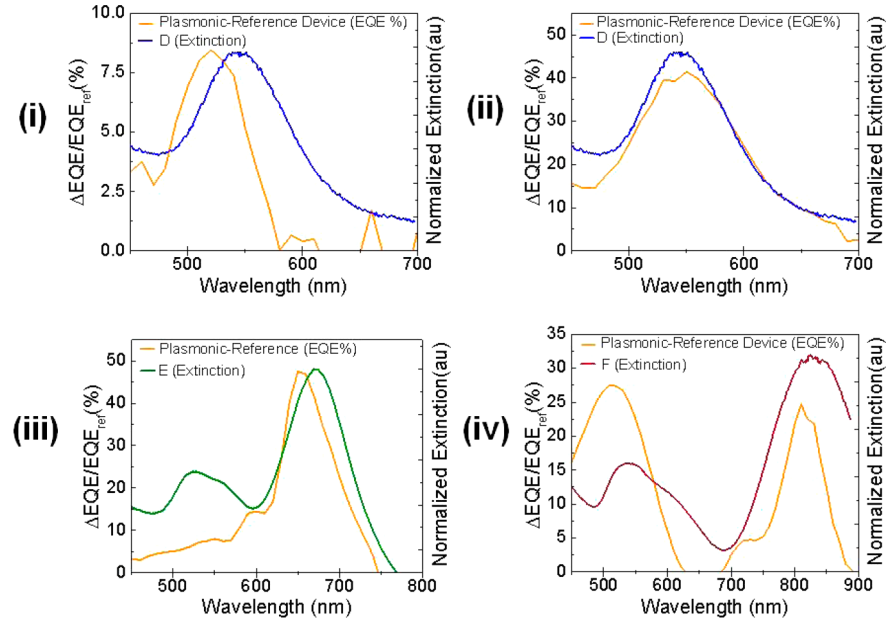

Figure 2. Spectral EQE enhancements of (i) P3HT-based device with Au/SiO_2 nanospheres (solution D). (ii) PBDTT-DPP-based device with solution Au/SiO_2 nanospheres (solution D). (iii) P3HT-based device with AR ~ 2.5 Au/SiO_2 core/shell nanorods (solution E). (iv) PBDTT-DPP-based device with AR ~ 4 Au/SiO_2 core/shell nanorods (solution F).

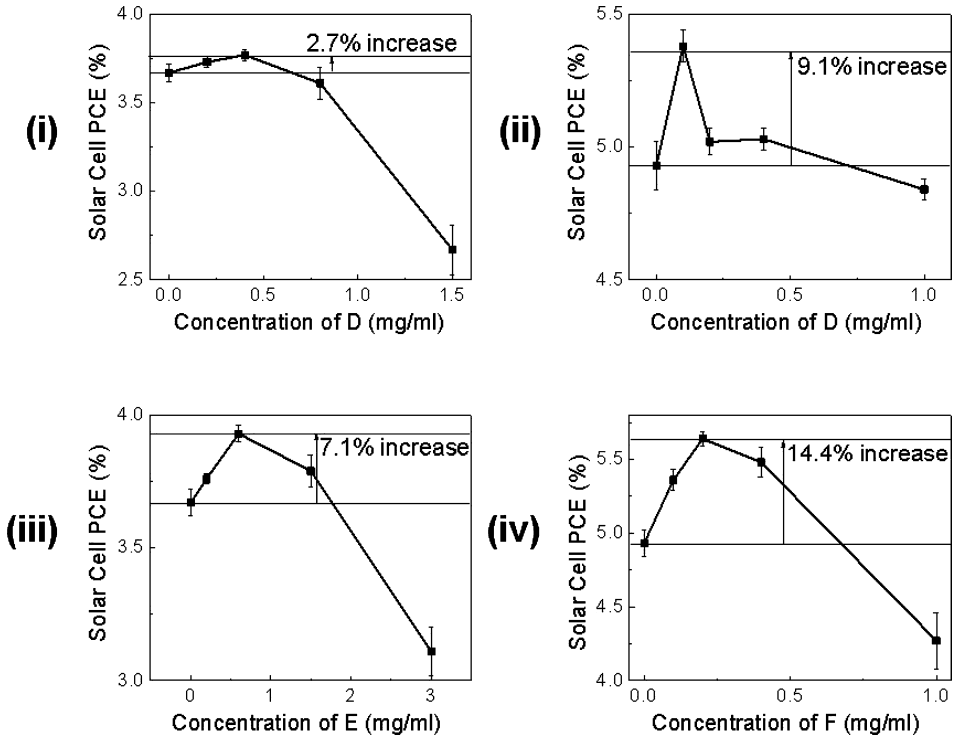

Figure 3. Solar cell PCE as a function of Au/SiO_2 nanosphere and nanorod concentrations for (i) D in P3HT:$PC_{60}BM$, (ii) D in PBDTT-DPP:$PC_{60}BM$, (iii) E in P3HT:$PC_{60}BM$, and (iv) F in PBDTT-DPP:$PC_{60}BM$.

0.2 mg/mL for the AR ~ 4 Au/SiO_2 nanorods; concentrations of either nanospheres or nanorods greater than 1 mg/mL resulted in OPV device performance degradation. The results of the concentration study are summarized in Figure 3.

We postulate that the reason for the observed trends is that, with increasing Au/SiO_2 core/shell nanoparticle concentration, the OPV cell morphology is disturbed. In order to investigate this further, atomic force microscopy (AFM) studies of the surfaces of the OPV cells with Au/SiO_2 core/shell nanospheres that yielded the highest and lowest PCEs along with reference devices for both the P3HT and PBDTT-DPP-based OPV devices were conducted using a Bruker Dimension 5000 scanning probe microscope (SPM) in "tapping" mode. The best plasmonic OPV devices show similar height and phase images as the reference devices, indicating a relatively unchanged morphology in the bulk heterojunction. On the other hand, the plasmonic OPV devices with higher Au nanorod loading show increased roughness as well as some abrupt bumps on the surface, which might be the aggregations of the Au/SiO_2 nanoparticles. Figures S.1 and S.2 in the Supporting Information show the results of our AFM study. The BHJ morphology evolution as with different addition of Au/SiO_2 nanoparticles is certainly a critical factor affecting the overall device performance; for example, the Au/SiO_2 nanoparticles might alter the crystallinity, molecular packing, and donor/acceptor interface. However, the detailed morphology study is beyond the scope of this work.

CONCLUSION

In conclusion, we achieved improvements in the PCE and J_{sc} of two OPV polymer systems by incorporating resonant light absorption and scattering Au/SiO_2 core/shell nanorods in their active regions. For the P3HT:$PC_{60}BM$ system, the incorporation of Au/SiO_2 core/shell nanospheres with a peak extinction wavelength of ~540 nm into the active layer led to a 2.7% increase in PCE. Active layer incorporation of Au/SiO_2 nanorods with a peak extinction wavelength of ~670 nm matching the P3HT:$PC_{60}BM$ polymer band edge led to a 7.1% increase in OPV device PCE. For the PBDTT:$PC_{60}BM$ system, active layer incorporation of Au/SiO_2 nanospheres with a peak extinction wavelength of ~540 nm led to a 9.1% increase in PCE, while Au/SiO_2 core/shell nanorods with a peak extinction wavelength of ~830 nm matching the band edge of PBDTT-DPP:$PC_{60}BM$ showed the highest PCE enhancement, a 14.4% increase. The results indicate that spectral tuning of the active layer plasmonic light trapping particles is a key consideration for plasmonic light trapping in OPVs. In order to maximize light trapping in practical applications, the extinction peak wavelength of active layer-incorporated Au/SiO_2 nanoparticles should spectrally match wavelength regions of poor OPV light absorption. In spectral regions where the OPV polymer absorbs light efficiently, the effect of incorporating spectrally matched plasmonic light trapping nanoparticles was found to be less pronounced.

Our data also indicate that plasmonic OPV device performance is sensitive to the Au/SiO_2 core/shell nanoparticle concentration incorporated into the active layer. Device performance was found to increase with the addition of core/shell nanoparticles up to a certain concentration; higher concentrations of core/shell nanoparticles were found to degrade device performance. AFM analysis indicated that the addition of high concentrations of Au/SiO_2 core/shell particles in the active layer led to the increased surface roughness and potential disruption of the OPV polymer morphology.

The results of this study support the viability of our approach of increasing OPV solar cell device efficiencies by incorporating spectrally tuned Au/SiO_2 core/shell nanorods into OPV active layers. Our data indicate that plasmonic enhancement should target spectral regions where the OPV cell absorbs poorly and that the concentration of the plasmonic light trapping nanoparticles should be carefully controlled.

METHODS

Au/SiO_2 Core/Shell Nanoparticle Synthesis. The synthesis of Au nanospheres was achieved by reducing gold chloride ($HAuCl_4$) with sodium borohydride ($NaBH_4$) in the presence of a surfactant (cetyltrimethylammoniumbromide (CTAB)). To prepare 10.6 mL of Au nanospheres, 5 mL of a 0.5 mM $HAuCl_4$ solution was mixed with 5 mL of a 0.2 M CTAB solution, and then 0.6 mL of ice cold $NaBH_4$ was added to initiate the reaction. The protocol produces 2−5 nm diameter nanospheres which increased in size to ∼20 nm diameter nanospheres over a few days.

Synthesis of Au nanorods required preparation of two solutions: a seed solution and a growth solution. The seed solution was prepared by mixing 5 mL of 0.5 mM $HAuCl_4$, 5 mL of 0.2 M CTAB, and 0.6 mL of 0.1 M ice cold $NaBH_4$. A solution of nanorods with a plasmon resonance of ∼650 nm was prepared using a growth solution that contained 0.6 mL of 0.01 M $AgNO_3$, 20 mL of 0.5 mM $HAuCl_4$, 20 mL of 0.2 M CTAB, and 0.7 mL of 0.77 M ascorbic acid. To prepare nanorods with an extinction peak of ∼800 nm, 0.9 mL of 0.01 M $AgNO_3$ was used instead of 0.6 mL of 0.01 M $AgNO_3$ in the growth solution. The growth process was initiated by injecting 26 μL of seed solution into the growth solution at a temperature of 27 °C. The reaction took approximately 2 h to come to completion.

To coat the Au nanorods with SiO_2, a literature protocol developed by Pastoriza-Santos was followed.[43] The nanorods were first rendered vitreophyllic by treating them with consecutive polyelectrolyte layers. Au metal has little affinity for SiO_2 because, unlike most other metals, it does not form a passivating oxide film in solution. Furthermore, the CTAB stabilizing surfactant interferes with the SiO_2 coating process. In order to replace the CTAB stabilizer and modify the Au nanorod surface chemistry, consecutive polyelectrolyte layers were adsorbed onto the metal surface. This process proceeded in the following manner. First, the as-synthesized, CTAB-stabilized Au rods were centrifuged, and the precipitate was redissolved in 3 mL of distilled water and then added to 3 mL of an aqueous solution containing polystyrene sulfonate (PSS) (2 mg/mL and 6 mM NaCl) and stirred for approximately 3 h. The PSS-modified particles were centrifuged twice to remove any excess PSS and redispersed in 3 mL of deionized water. The dispersion was then added dropwise under vigorous stirring to 3 mL of an aqueous solution of poly(aniline hydrochloride) (PAH) of (2 mg/mL and 6 mM NaCl). PAH adsorption was allowed to proceed for 3 h. The sample was then centrifuged to remove excess polyelectrolyte and redispersed in 3 mL of deionized water. Finally, 3 mL of the PSS/PAH-functionalized Au spheres was added to a polyvinylpyrrolidone (PVP) solution (4 mg/mL). The mixture was stirred for approximately 12 h, centrifuged to remove any excess polymer, and redispersed in 0.2 mL of deionized water. This aqueous dispersion of PVP-coated nanoparticles was then added dropwise and under vigorous stirring to 2 mL of isopropyl alcohol (IPA). Once the Au nanoparticles were transferred into IPA, SiO_2 coating was completed through the adjustment of the pH and addition of tetraethylorthosilicate (TEOS). The pH was adjusted to 10 by adding 1.5 mL of 4 vol % NH_3 in IPA (27% in water). Finally, 0.4 mL of TEOS (1 vol % in ethanol) was added under gentle stirring, and the reaction was allowed to proceed for approximately 12 h.

In order to dissolve the Au/SiO_2 core/shell nanorods in an OPV-compatible solvent, such as dichlorobenzene, functionalization with OTMS was performed. The Au/SiO_2 core/shell nanorods were centrifuged and redissolved in 3 mL of ethanol containing 30 μL of NH_4OH (32%). Then, 300 μL of OTMS chloroform solution (3%) was added dropwise with vigorous stirring, and functionalization of the SiO_2 surface was achieved by hydrolysis of the methoxy groups and condensation of the resulting silane groups with SiOH groups on the SiO_2 surface. TEM using an FEI TF20 was used to confirm the morphology of the synthesized Au/SiO_2 core/shell nanorods, while UV−vis spectroscopy was used to determine the extinction spectra of the nanorod solutions.

Plasmonic OPV Device Fabrication. Polymer reference solutions consisted of 20 mg/mL of P3HT:$PC_{60}BM$ (1:1 weight ratio) and 6 mg/mL PBDTT-DPP:$PC_{60}BM$ (1:2.5 weight ratio). The plasmonic P3HT:$PC_{60}BM$ solar cell device solution was prepared by adding a solution of the OTMS-functionalized AR ∼ 2.5 Au/SiO_2 core/shell nanorods to the P3HT:$PC_{60}BM$ solution so that the final concentration of the nanorods was 0.6 mg/mL. The plasmonic PBDTT-DPP:$PC_{60}BM$ solar cell device solution was prepared by mixing the OTMS-functionalized AR ∼ 4 Au/SiO_2 core/shell nanorod solution with the PBDTT-DPP:$PC_{60}BM$ solution so that the final concentration of Au/SiO_2 core/shell nanorods was 0.2 mg/mL.

All of the devices in this article had the same structure: indium tin oxide (ITO)/ poly(ethylenedioxythiophene):polystyrenesulfonate (PEDOT:PSS) (4083)/active layer/calcium/aluminum. The PEDOT:PSS was precoated onto the ITO substrate and baked at 120 °C for 15 min before spin-casting the solutions. The P3HT:$PC_{60}BM$-based devices were spin-coated at 800 rpm for 40 s after which the wet films remained in the Petri dishes until they dried (the color of the films changed from orange to dark-red). This solvent annealing process has been demonstrated to attain an optimized morphology for P3HT:$PC_{60}BM$-based organic solar cell devices or organic photodetectors.[44,45] The PBDTT-DPP:$PC_{60}BM$-based devices were fabricated by spin-casting at 1800 rpm for 80 s with no other treatment. A bilayer cathode containing a Ca layer (20 nm) and a subsequent Al layer (100 nm) was deposited by thermal evaporation under high vacuum ($<3 \times 10^{-6}$ Torr). The active layer thickness of the P3HT:$PC_{60}BM$-based devices was ∼210 nm, while the thickness of the PBDTT-DPP:$PC_{60}BM$-based devices was ∼90 nm. The thickness was measured by a Vecoo Dektak 150 profiler.

Conflict of Interest: The authors declare no competing financial interest.

Acknowledgment. The authors would like to acknowledge the financial support received from the Office of Naval Research (Program Manager Dr. Paul Armistead, Fund Number N00014-11-1-0250), and the William F. Seyer Chair of UCLA. Technical

discussions with Dr. Gang Li and Dr. Benjamin Schwartz of UCLA were much appreciated.

Supporting Information Available: An expanded description of experimental procedures and characterizations is given. This material is available free of charge *via* the Internet at http://pubs.acs.org.

REFERENCES AND NOTES

1. Loutfy, R. O.; Sharp, J. H. Photovoltaic Properties of Metal-Free Phthalocyanines. I. Al/H_2Pc Schottky Barrier Solar Cells. *J. Chem. Phys.* **1979**, *71*, 1211–1217.
2. Morel, D. L.; Ghosh, A. K.; Feng, T.; Stogryn, E. L.; Purwin, P. E.; Shaw, R. F.; Fishman, C. High-Efficiency Organic Solar Cells. *Appl. Phys. Lett.* **1978**, *32*, 495–497.
3. Wagner, H. J.; Loutfy, R. O. Photoelectric Properties of CdS—MgPc Heterojunction Solar Cells. *J. Vac. Sci. Technol.* **1982**, *20*, 300–304.
4. Yokoyama, M.; Endo, Y.; Matsubara, A.; Mikawa, F. H. Mechanism of Extrinsic Carrier Photogeneration in Poly-*N*-vinylcarbazole. II. Quenching of Exciplex Fluorescence by Electric Field. *J. Chem. Phys.* **1981**, *75*, 3006–3011.
5. Yokoyama, M.; Shimokihara, S.; Matsubara, A.; Mikawa, H. Extrinsic Carrier Photogeneration in Poly-*N*-vinylcarbazole. III. CT Fluorescence Quenching by an Electric Field. *J. Chem. Phys.* **1982**, *76*, 724–728.
6. Tang, C. W. 2-Layer Organic Photovoltaic Cell. *Appl. Phys. Lett.* **1986**, *48*, 183–185.
7. Sariciftci, N. S.; Braun, D.; Zhang, C.; Srdanov, V. I.; Heeger, A. J.; Stucky, G.; Wudl, F. Semiconducting Polymer-Buckminsterfullerene Heterojunctions: Diodes, Photodiodes, and Photovoltaic Cells. *Appl. Phys. Lett.* **1993**, *62*, 585–587.
8. Sariciftci, N. S.; Smilowitz, L.; Heeger, A. J.; Wudl, F. Photoinduced Electron-Transfer from a Conducting Polymer to Buckminsterfullerene. *Science* **1992**, *258*, 1474–1476.
9. Hiramoto, M.; Fujiwara, H.; Yokoyama, M. P-I-N-like Behavior in Three-Layered Organic Solar Cells Having a Co-deposited Interlayer of Pigments. *J. Appl. Phys.* **1992**, *72*, 3781–3787.
10. Yu, G.; Gao, J.; Hummelen, J. C.; Wudl, F.; Heeger, A. J. Polymer Photovoltaic Cells: Enhanced Efficiencies *via* a Network of Internal Donor—Acceptor Heterojunctions. *Science* **1995**, *270*, 1789–1791.
11. Marks, R. N.; Halls, J. J. M.; Bradley, D. D. C.; Friend, R. H.; Holmes, A. B. The Photovoltaic Response in Poly(*p*-phenylene vinylene) Thin-Film Devices. *J. Phys.: Condens. Matter* **1994**, *6*, 1379–1383.
12. Goetzberger, A.; Hebling, C.; Schock, H. W. Photovoltaic Materials, History, Status and Outlook. *Mater. Sci. Eng. Rep.* **2003**, *40*, 1–46.
13. Li, W. W.; Zhou, Y.; Andersson, B. V.; Andersson, L. M.; Thomann, Y.; Veit, C.; Tvingstedt, K.; Qin, R. P.; Bo, Z. S.; Inganas, O.; *et al.* The Effect of Additive on Performance and Shelf-Stability of HSX-1/PCBM Photovoltaic Devices. *Org. Electron.* **2011**, *12*, 1544–1551.
14. Duong, D. T.; Walker, B.; Lin, J.; Kim, C.; Love, J.; Purushothaman, B.; Anthony, J. E.; Nguyen, T. Q. Molecular Solubility and Hansen Solubility Parameters for the Analysis of Phase Separation in Bulk Heterojunctions. *J. Polym. Sci., Part B: Polym. Phys.* **2012**, *50*, 1405–1413.
15. Fang, G.; Liu, J.; Fu, Y. Y.; Meng, B.; Zhang, B. H.; Xie, Z. Y.; Wang, L. X. Improving the Nanoscale Morphology and Processibility for PCDTBT-Based Polymer Solar Cells *via* Solvent Mixtures. *Org. Electron.* **2012**, *13*, 2733–2740.
16. Song, Y.; Ryu, S. O. The Effect of Solvent Systems on the Electrical Performance of P3HT:PCBM-C61 Photoactive Layers. *J. Nanoelectron. Optoelectron.* **2012**, *7*, 549–553.
17. Ma, W.; Yang, C.; Gong, X.; Lee, K.; Heeger, A. J. Thermally Stable, Efficient Polymer Solar Cells with Nanoscale Control of the Interpenetrating Network Morphology. *Adv. Funct. Mater.* **2005**, *15*, 1617–1622.
18. Brady, M. A.; Su, G. M.; Chabinyc, M. L. Recent Progress in the Morphology of Bulk Heterojunction Photovoltaics. *Soft Matter* **2011**, *7*, 11065–11077.
19. Padinger, F.; Rittberger, R. S.; Sariciftci, N. S. Effects of Postproduction Treatment on Plastic Solar Cells. *Adv. Funct. Mater.* **2003**, *13*, 85–88.
20. Dou, L.; You, J.; Yang, J.; Chen, C. C.; He, Y.; Murase, S.; Yang, Y. Tandem Polymer Solar Cells Featuring a Spectrally Matched Low-Bandgap Polymer. *Nat. Photonics* **2012**, *6*, 180–185.
21. Service, R. F. Outlook Brightens for Plastic Solar Cells. *Science* **2011**, *332*, 293–295.
22. You, J.; Dou, L.; Yoshimura, K.; Kato, T.; Ohya, K.; Moriarty, T.; Yang, Y. A Polymer Tandem Solar Cell with 10.6% Power Conversion Efficiency. *Nat. Commun.* **2013**, *4*, 1446.
23. Li, G.; Zhu, R.; Yang, Y. Polymer Solar Cells. *Nat. Photonics* **2012**, *6*, 153–161.
24. Park, S. H.; Roy, A.; Beaupre, S.; Cho, S.; Coates, N.; Moon, J. S.; Moses, D.; Leclerc, M.; Lee, K. Bulk Heterojunction Solar Cells with Internal Quantum Efficiency Approaching 100%. *Nat. Photonics* **2009**, *3*, 297–302.
25. Deckman, H. W.; Roxlo, C. B.; Yablonovitch, E. Maximum Statistical Increase of Optical Absorption in Textured Semiconductor Films. *Opt. Lett.* **1983**, *8*, 491–493.
26. Battaglia, C.; Hsu, C.-M.; Söderström, K.; Escarré, J.; Haug, F.-J.; Charrière, M.; Boccard, M.; Despeisse, M.; Alexander, D. T. L.; Cantoni, M.; *et al.* Light Trapping in Solar Cells: Can Periodic Beat Random? *ACS Nano* **2012**, *6*, 2790–2797.
27. Atwater, H. A.; Polman, A. Plasmonics for Improved Photovoltaic Devices. *Nature* **2010**, *9*, 205–213.
28. Qiaoqiang, G.; Bartoli, F. J.; Kafafi, Z. H. Research Highlights on Organic Photovoltaics and Plasmonics. *IEEE Photonics J.* **2012**, *4*, 620–624.
29. Huang, X.; Neretina, S.; El-Sayed, M. A. Gold Nanorods: From Synthesis and Properties to Biological and Biomedical Applications. *Adv. Mater.* **2009**, *21*, 4880–4910.
30. Chen, H.; Shao, L.; Li, Q.; Wang, J. Gold Nanorods and their Plasmonic Properties. *Chem. Soc. Rev.* **2013**, *42*, 2679–2724.
31. Catchpole, K. R.; Polman, A. Plasmonic Solar Cells. *Opt. Express* **2008**, *16*, 21793–21800.
32. Spinelli, P.; Ferry, V. E.; Groep, J. V. D.; Lare, M. V.; Verschuuren, M. A.; Schropp, R. E. I.; Atwater, H. A.; Polman, A. Plasmonic Light Trapping in Thin-Film Si Solar Cells. *J. Opt.* **2012**, *14*, 024002–024013.
33. Morfa, A. J.; Rowlen, K. L.; Reilly, T. H.; Romero, M. J.; van de Lagemaat, J. Plasmon-Enhanced Solar Energy Conversion in Organic Bulk Heterojunction Photovoltaics. *Appl. Phys. Lett.* **2008**, *92*, 13504–13505.
34. Qiao, L.; Wang, D.; Zuo, L.; Ye, Y.; Qian, J.; Chen, H.; He, S. Localized Surface Plasmon Resonance Enhanced Organic Solar Cell with Gold Nanospheres. *Appl. Energy* **2011**, *88*, 848–852.
35. Wu, J. L.; Chen, F. C.; Hsiao, Y. S.; Chien, F. C.; Chen, P.; Kuo, C. H.; Huang, M. H.; Hsu, C. S. Surface Plasmonic Effects of Metallic Nanoparticles on the Performance of Polymer Bulk Heterojunction Solar Cells. *ACS Nano* **2011**, *5*, 959–967.
36. Yang, J.; You, J. B.; Chen, C. C.; Hsu, W. C.; Tan, H. R.; Zhang, X. W.; Hong, Z. R.; Yang, Y. Plasmonic Polymer Tandem Solar Cell. *ACS Nano* **2011**, *5*, 6210–6217.
37. Lee, J. Y.; Peumans, P. The Origin of Enhanced Optical Absorption in Solar Cells with Metal Nanoparticles Embedded in the Active layer. *Opt. Express* **2010**, *18*, 10078–10087.
38. Qu, D.; Liu, F.; Huang, Y.; Xie, W.; Xu, Q. Mechanism of Optical Absorption Enhancement in Thin Film Organic Solar Cells with Plasmonic Metal Nanoparticles. *Opt. Express* **2011**, *19*, 24795–24803.
39. Szeremeta, J.; Nyk, M.; Chyla, A.; Strek, W.; Samoc, M. Enhancement of Photoconduction in a Conjugated Polymer through Doping with Copper Nanoparticles. *Opt. Mater.* **2011**, *33*, 1372–1376.
40. Wang, D. H.; Kim, D. Y.; Choi, K. W.; Seo, J. H.; Im, S. H.; Park, J. H.; Park, O. O.; Heeger, A. J. Enhancement of Donor—Acceptor Polymer Bulk Heterojunction Solar Cell Power Conversion Efficiencies by Addition of Au Nanoparticles. *Angew. Chem., Int. Ed.* **2011**, *50*, 5519–5523.

41. Xue, M.; Li, L.; Tremolet de Villers, B. J.; Shen, H.; Zhu, J.; Yu, Z.; Stieg, A. Z.; Pei, Q.; Schwartz, B. J.; Wang, K. L. Charge-Carrier Dynamics in Hybrid Plasmonic Organic Solar Cells with Ag Nanoparticles. *Appl. Phys. Lett.* **2011**, *98*, 3302–3305.
42. Huang, X.; Jain, P. K.; El-Sayed, I. H.; El-Sayed, M. A. Gold Nanoparticles: Interesting Optical Properties and Recent Applications in Cancer Diagnostic and Therapy. *Nanomedicine* **2007**, *2*, 681–693.
43. Pastoriza-Santos, I.; Perez-Juste, J.; Liz-Marzan, L. M. Silica-Coating and Hydrophobation of CTAB-Stabilized Gold Nanorods. *Chem. Mater.* **2006**, *18*, 2465–2467.
44. Li, G.; Shrotriya, V.; Huang, J.; Yao, Y.; Moriarty, T.; Emery, K.; Yang, Y. High-Efficiency Solution Processable Polymer Photovoltaic Cells by Self-Organization of Polymer Blends. *Nat. Mater.* **2005**, *4.11*, 864–868.
45. Yang, Y.; Zhong, H.; Bai, Z.; Zou, B.; Li, Y.; Scholes, G. D. Transition from Photoconductivity to Photovoltaic Effect in P3HT/$CuInSe_2$ Composites. *J. Phys. Chem. C* **2012**, *116*, 7280–7286.